Measurement 230 (2024) 114520

Contents lists available at ScienceDirect

Measurement

journal homepage: www.elsevier.com/locate/measurement

Distributed strain monitoring method for structural vibration based on multi-point acceleration measurement

Huang Xinjing, Zhang Zhipeng, Cheng Tongyao, Li Jian, Ma Jinyu *

State Key Laboratory of Precision Measurement Technology and Instruments, Tianjin 300072, China

ARTICLE INFO

Keywords:
FBG
Vibration monitoring
Deformation
Displacement
Pipeline

ABSTRACT

Fiber Bragg Grating (FBG) has been widely used in vibration monitoring due to its advantages of high sensitivity, resistance to electromagnetic interference and ease of networking. This paper proposes a method of distributed strain monitoring for vibrating structures where the surface is unsuitable for attaching FBG. This method utilizes measured multi-point acceleration to calculate dynamic displacement, and subsequently reconstructs distributed strain based on displacement matching and a displacement–strain function. Finite element simulation results demonstrate that the displacement matching scheme has higher strain reconstruction accuracy and broader adaptability. An FBG accelerometer with an equal-strength beam is designed, fabricated, and tested, exhibiting a resonant frequency of 56 Hz and an average sensitivity of 70 pm·g^{-1} in the flat frequency band. The proposed method is experimentally validated using a 12 m steel pipeline. It's demonstrated that the displacement reconstruction error is less than 8 %, and the strain reconstruction error is less than 11 %.

1. Introduction

In practical engineering applications, large structures such as rails, pipelines, and bridges often experience low-frequency vibrations due to manufacturing defects or external load influences [1,2]. The low-frequency vibrations can accelerate the structure's fatigue and wear, potentially leading to structural failure, deformation and serious accidents [3]. Therefore, monitoring the vibration characteristics of the structure and obtaining timely and accurate information regarding its displacement and strain are of great significance [4].

One class of vibration shape monitoring methods adopts electrical sensing principles, such as piezoelectric accelerometer [5], capacitive sensor [6] and resistance strain gauge [7]. These methods suffer from significant signal conversion and transmission losses, as well as susceptibility to electromagnetic interference, making it difficult to achieve large-scale remote monitoring. In contrast, optical fiber sensors have the characteristics of strong toughness, corrosion resistance, small diameter, strong flexibility and deformability, and can be used for vibration monitoring in complex environments [8]. Optical signals transmitted through optical fibers are affected by the external environment, and by analyzing the changes in optical signal characteristics, external environmental parameters can be obtained [8–10]. The fiber optic strain sensors generally include the following five types: FBG sensors, intensity-based sensors, multimodal interference-based sensors, Brillouin-frequency-based sensors, and Fabry-Perot cavity sensors [11]. Among them, Brillouin-frequency-based sensors and FBG sensors are the most widely used in civil structure health monitoring [12]. The former is limited to static condition due to the essential long acquisition time of the frequency sweep process, while latter has the advantage of being applicable to dynamic and quasi-distributed monitoring scenarios [12]. With high resolution, high frequency bandwidth, and ease of configuring diverse sensing networks, FBG sensors have been widely used in the field of structural vibration shape monitoring [13].

There are two methods of vibration shape monitoring: displacement reconstruction using FBG strainmeters [14–16] and strain reconstruction using FBG accelerometers [17–19]. The FBG strainmeter requires the grating region or both ends of the FBG to be firmly connected with the structure to be monitored [15], ensuring that the strain of the FBG is equal to or proportional to the surface strain of the structures such as aircraft [20] and ship hulls [21]. For structures where FBG strainmeters cannot be directly affixed onto the surface or the adhesive cannot stably transfer strain, FBG accelerometers can be used to reconstruct the vibration displacement for risk assessment. Lee et al. [17] proposed a new scheme to reconstruct displacement using measured acceleration by minimizing the squared error between measured acceleration and approximate acceleration. Zheng W et al [18] proposed a real-time

* Corresponding author.
E-mail address: jinyu.ma@tju.edu.cn (M. Jinyu).

https://doi.org/10.1016/j.measurement.2024.114520
Received 28 May 2023; Received in revised form 15 March 2024; Accepted 16 March 2024
Available online 26 March 2024

displacement reconstruction method using baseline correction technology, which can reduce the error trend term in the integration process of acceleration signal. Zhu et al. [19] used the Low Frequency Attenuation (LFA) algorithm to integrate acceleration signals in the frequency domain to reconstruct displacement. Displacement can indicate vibration magnitude, but cannot directly indicate the fracture risk of the structure– which can be achieved by reconstructing the distributed strain using displacement information. However, the above studies did not study how to reconstruct the displacement by using multi-point acceleration and then reconstruct the distributed strain by using displacement information.

For these methods of vibration displacement reconstruction, FBG accelerometer is the most critical sensing unit. FBG accelerometers can be classified into spring oscillator structures [22,23], elastic diaphragm structures [24,25] and cantilever beam structures [26–29]. Among these, the cantilever beam FBG accelerometer has been widely used due to its strong resistance to lateral interference, high sensitivity, and ease of fabrication [30–32]. The cantilever FBG accelerometer can employ equal cross-section cantilever beam or equal strength beam structures [33]. The FBG on the equal strength beam can be uniformly stretched, so the characteristic peak of the spectrum is more noticeable for accurate strain characterization.

This paper proposes a displacement–strain reconstruction method based on FBG accelerometers for the scenarios where FBG strainmeters cannot be directly attached to the structure surface. First, displacement reconstruction algorithm using acceleration on multiple points is studied and then verified through simulation. Second, the distributed strain reconstruction of a pipe beam is tested using the reconstructed displacement via finite element simulation, where two methods are employed: displacement–strain function and displacement matching via finite element simulation. Third, based on the sensing principle of FBG, a FBG accelerometer with an equal strength beam structure is developed. Lastly, experiment is carried out to verify the feasibility of the proposed method on a steel pipeline simply supported at both ends.

2. Distributed strain reconstruction

2.1. Reconstruction scheme

In the process of monitoring structural vibration shape, the displacement and strain of the structure are the key indicators for evaluating its safety status. A scheme is designed to measure the displacement and strain of the structure, particularly in cases where the surface of the structure is relatively rough and the FBG strainmeter cannot be directly attached. The acceleration at several discrete points is measured by the FBG accelerometer array fixed on the structure, and the displacement reconstruction algorithm is used to obtain the displacement at each point. The distributed strain of the structure is calculated using the displacement–strain function derived from vibratory beam theory and displacement matching via finite element simulation. Then the feasibility and accuracy of these two methods for monitoring structural vibration shape are compared through simulation and the adaptability is analyzed.

2.2. Dynamic displacement reconstruction

The displacement reconstruction algorithm based on Finite Impulse Response (FIR) filter is used to calculate displacement by using a linear combination of accelerations in a finite time interval. The principle is approximated by a FIR filter, which effectively suppresses low-frequency noise and eliminates trend terms in the signal. This method minimizes the squared error between the measured acceleration and the second-order central finite difference of the displacement and overcomes the problem caused by the lack of boundary conditions in the time window by using the Tikhonov regularization scheme. As shown in equation (1), the acceleration $a(t)$ of a measurement point can be represented by a second-order ordinary differential equation of the displacement $u(t)$. If the displacement or velocity boundary conditions at $t = T_1$ or $t = T_2$ are known, the displacement can be obtained by integrating equation (1) twice.

$$a(t) \equiv \frac{d^2u(t)}{dt^2},\ T_1 < t < T_2\# \tag{1}$$

However, the boundary conditions are usually unknown, the minimization method is used to avoid solving the equation directly. The specific principles are outlined as follows [17].

The calculated acceleration a_p at the discrete point can be expressed through second-order central finite difference of the displacement u_p, which is the proper approximation of the equation (1):

$$\frac{u_{p+1} - 2u_p + u_{p-1}}{(\Delta t)^2} = a_p p = 1, \cdots, 2k+1\# \tag{2}$$

wherein u_p is the displacement at the p-th time step as shown in Figs. 1, and 2 $k + 1$ is the number of data points in duration of time $T_1 \le t \le T_2$.

Eq. (2) can be rewritten in the form of matrices for all time steps:

$$\frac{1}{(\Delta t)^2}\mathbf{L}_c u = a\# \tag{3}$$

wherein $\mathbf{L_c}$ is $(2k + 1) \times (2k + 3)$ order linear operator matrix, and $\mathbf{u}$ is the displacement vector of discrete time steps.

$$\mathbf{L_c} = \begin{bmatrix} 1 & -2 & 1 & & & & \\ & 1 & -2 & 1 & & 0 & \\ & & & \ddots & & & \\ & 0 & & 1 & -2 & 1 & \\ & & & & 1 & -2 & 1 \end{bmatrix},\quad \mathrm{u} = \begin{bmatrix} u_0 \\ u_1 \\ \vdots \\ u_{k+1} \\ \vdots \\ u_{2k+1} \\ u_{2k+2} \end{bmatrix}\# \tag{4}$$

Within the time window, the minimization problem can be expressed as:

$$\underset{u}{Min} E_a(u) = \frac{1}{2}\int_{T_1}^{T_2} (a(t) - \widetilde{a}(t))^2\, dt\# \tag{5}$$

wherein $\widetilde{a}(t)$ represent measured acceleration. Eq. (5) can be discretized into Eq. (6) through the trapezoidal rule:

$$\underset{u}{Min} E_a(u) \approx \frac{1}{2}\left(\frac{1}{2}(a_1 - \overline{a}_1)^2 + \cdots + (a_{2k} - \overline{a}_{2k})^2 \quad + \frac{1}{2}(a_{2k+1} - \overline{a}_{2k+1})^2\right)\Delta t \tag{6}$$

The above equation can be expressed in matrixs as:

$$\underset{u}{Min} E_a(u) = \frac{1}{2}(\mathbf{a} - \widetilde{\mathbf{a}})^T(\mathbf{L_a})^T\mathbf{L_a}(\mathbf{a} - \widetilde{\mathbf{a}})\Delta t$$

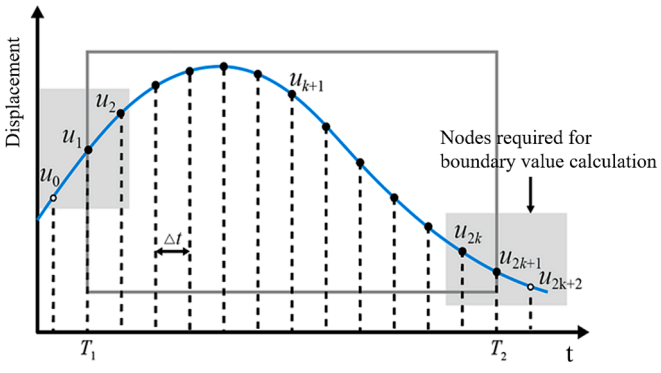

Fig. 1. The displacements at discrete time steps.

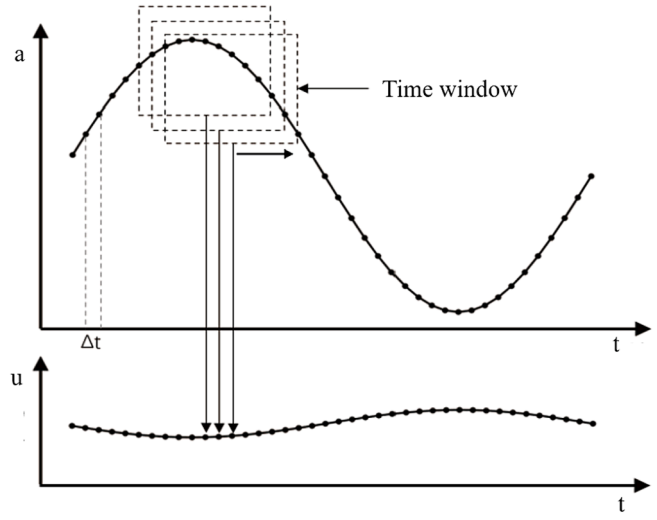

Fig. 2. Displacement reconstruction process based on overlapping moving windows.

$$= \frac{1}{2}\|\mathbf{L}_\mathbf{a}(\mathbf{a} - \tilde{\mathbf{a}})\|_2^2 \Delta t \# \tag{7}$$

wherein $||\bullet||$ is the 2-norm of the vector, and $\mathbf{L_a}$ is the diagonal weighted matrix of order $(2k+1)$, corresponding to the maximum subscript value of acceleration.

$$\mathbf{L}_\mathbf{a} = \begin{bmatrix} \frac{1}{\sqrt{2}} & & & 0 \\ & 1 & & \\ & & \ddots & \\ & & & 1 \\ 0 & & & \frac{1}{\sqrt{2}} \end{bmatrix}_{(2k+1)(2k+1)} \# \tag{8}$$

Substituting Eq. (3) into Eq. (7), one can get the expression:

$$\underset{u}{Min} E_a(u) = \frac{1}{2}\|\mathbf{Lu} - (\Delta t)^2 \mathbf{L}_\mathbf{a}\tilde{\mathbf{a}}\|_2^2 \# \tag{9}$$

wherein $\mathbf{L} = \mathbf{L_a}\mathbf{L_c}$. For $(2k+3)$ unknown displacements, only $(2k+1)$ finite difference equations are defined, which means $\mathbf{L}$ is not a full rank matrix, and a unique displacement solution cannot be obtained from the measured acceleration. By providing two boundary conditions to Eq. (9) and using these conditions to define the other two equations, the minimization problem can be solved.

The regularization function R is used to define the boundary of the solution:

$$R = \frac{1}{2}\|\mathbf{u}\|_2^2 \le r^2 < \infty \# \tag{10}$$

wherein r is a constant and unknown. The regularity condition Eq. (10) is used as a penalty function for the minimization problem:

$$\underset{u}{Min} E_a'(u) = \frac{1}{2}\|\mathbf{Lu} - (\Delta t)^2 \mathbf{L}_\mathbf{a}\tilde{\mathbf{a}}\|_2^2 + \frac{\lambda^2}{2}\|\mathbf{u}\|_2^2 \# \tag{11}$$

The above problem is referred to as Tikhonov regularization methods. Wherein,λ is usually called regularization factor, which is used to adjust the degree of regularization in the minimization problem, and λ is defined as follows:

$$\lambda = 46.81 N_d^{-1.95} \# \tag{12}$$

wherein N_d is the number of data points in the time window, and when the average size of the time window is three times the maximum period of acceleration data acquisition, the optimal regularization factor is accurate enough.The solution of Eq. (11) can be given as:

$$u = \left(\mathbf{L}^\mathbf{T}\mathbf{L} + \lambda^2\mathbf{I}\right)^{-1}\mathbf{L}^\mathbf{T}\mathbf{L}_\mathbf{a}\tilde{\mathbf{a}}(\Delta t)^2 = \mathbf{C}_\mathbf{a}\tilde{\mathbf{a}}(\Delta t)^2 \# \tag{13}$$

The estimated displacement in Eq. (13) has an increasing error near the boundary (i.e. the starting and ending points of **u**), resulting in a decrease in computational accuracy. To address this issue, overlapping moving window technology is used. For each time window shown in Fig. 2, the displacement is calculated using Eq. (13), but only the reconstructed displacement at the center of each time window is used as the estimated displacement. The time window is then shifted forward by Δt and the same process is repeated to obtain the displacements at points other than the boundary.

2.3. Vibration equation of the beam

The acceleration measured by the FBG accelerometers can be used to obtain the displacement of discrete points through a dynamic displacement reconstruction algorithm. In order to monitor the strain of the structure, it is necessary to study the relationship between structural displacement and strain. When the main deformation of the beam is bending deformation, the influence of shear deformation and the moment of inertia of the section around the neutral axis can be ignored during low-frequency vibration.

As shown in Fig. 3, let the density of the beam material be the cross-sectional area be A. The micro segment beam dx is taken, and the bending moment and shear force on the section are M and F_s, respectively. $y = y(x, t)$ represents the lateral displacement of the beam, which is a function of the cross-sectional position x and time t. Assuming the interference force $f = 0$ N, the motion equation of the micro segment beam is given by:

$$\frac{\partial^2}{\partial x^2}\left(EI\frac{\partial^2 y}{\partial x^2}\right) = -\rho A\frac{\partial^2 y}{\partial t^2} \# \tag{14}$$

wherein E is the elastic modulus of the beam, and I is the moment of inertia of the section. For beams with equal cross-section, E, I, ρ are constants.

Using the variable separation method to solve Eq. (14) and assuming $y(x,t) = Y(x)F(t)$, we obtain:

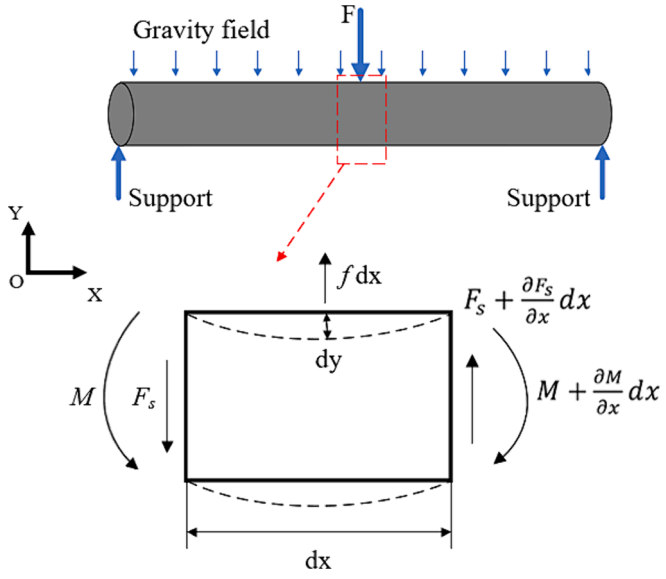

Fig. 3. Stress analysis of micro segment beam.

$$\frac{\ddot{F}(t)}{F(t)} = -\frac{d^2\left[\frac{d^2Y(x)}{dx^2}\right]}{\frac{EI}{\rho AY(x)}} = -\omega^2 \# \tag{15}$$

wherein ω is the angular frequency of vibration, and then,

$$\frac{d^4Y(x)}{dx^4} = \beta^4 Y(x) \# \tag{16}$$

wherein $\beta^4 = \rho A\omega^2/EI$. According to Eq. (16), the displacement of the beam can be obtained as:

$$Y(x) = C_1 cos(\beta x) + C_2 sin(\beta x) + C_3 ch(\beta x) + C_4 sh(\beta x) \# \tag{17}$$

According to the boundary conditions of the simply supported beams, the corresponding modal functions of each order during the free vibration process can be solved as:

$$Y_i(x) = sin(\frac{i\pi}{L}x)(i = 1, 2, \cdots) \# \tag{18}$$

wherein L is the length of the simply supported beam. By using Eq. (18), the displacement of discrete points at a certain time can be fitted as a continuous displacement curve for subsequent strain calculations.

2.4. Displacement-strain reconstruction

Method 1: using displacement–strain function

According to the principles of material mechanics, if the distance from the surface of the beam to the neutral layer is h, the relationship between its displacement and strain can be expressed by the following equation:

$$\varepsilon(x) = \frac{h}{2}\frac{d^2Y(x)}{dx^2} \# \tag{19}$$

The strain is proportional to the second derivative of the vibration displacement function of the beam, and the vibration displacement function of the beam can be obtained by fitting displacement of discrete points. Then the strain distribution of the beam can be calculated according to equation (19).

Method 2: displacement matching via finite element simulation

Finite element simulation is used to model the structure vibration, and the vibration displacement distribution curves at each time can be obtained through transient simulation study. The displacement reconstruction algorithm is executed to reconstruct the displacements using the acceleration data of each FBG accelerometer at the measurement points. The reconstructed displacements of discrete points are matched with the vibration displacement curves at each moment in the simulation, and the simulated strain at a certain moment with the smallest error is selected as the final distributed strain of the structure.

3. Simulation verification

3.1. Strain reconstruction based on displacement–strain function

The simulation modeling is shown in Fig. 4. Instantaneous force F is applied to the center of the simply supported pipeline to generate vibration. Seven measuring points are symmetrically distributed on two sides of the pipeline. The displacement curve and strain curve obtained from finite element simulation are taken as reference.

MATLAB fitting toolbox is used to fit the pipeline displacement data at those discrete points using Eq. (18). The fitting result is shown as Eq. (20), and the comparison curve between the fitted displacement and the reference displacement is depicted in Fig. 5.

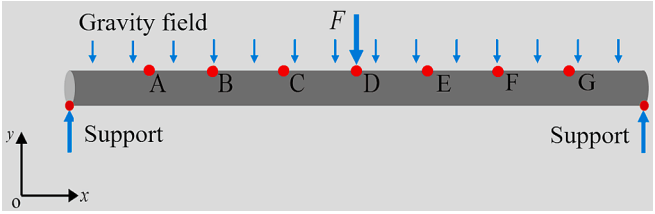

Fig. 4. Simulation model for displacement–strain reconstruction of a simply supported pipeline.

$$Y(x) = -0.0883\sin\left(\frac{\pi x}{12}\right) \# \tag{20}$$

According to Eq. (19), the strain distribution function of the pipeline at $t = 1$ s can be calculated as:

$$\varepsilon(x) = -326.8\sin(\frac{\pi x}{12}) \# \tag{21}$$

Eq. (21) is the expression for microstrain με. The strain distribution curve is drawn according to Eq. (21) and compared with the reference strain curve, as shown in Fig. 6. It is evident that the strain distribution obtained from simulation is basically consistent with the reconstructed results. However, when the shape of the beam and the supporting conditions are complicated, the exact analytical solution of the vibration equation of the beam cannot be obtained. Therefore, it is usually difficult to accurately calculate the actual strain according to the beam vibration theory because of the differences between actual measurement conditions and ideal conditions. This method is particularly suitable for vibration monitoring of simple beams.

3.2. Strain reconstruction based on displacement matching

The simulation model is identical to that shown in Fig. 4. First, the initial displacement of the pipeline when the applied force $F = 0$ N and the vibration displacement curves within 0–5 s of the pipeline are recorded, as shown in Fig. 7. The time interval between the curves in the figure is 6.25 ms. Due to the negative initial displacement of the pipeline and the small applied force F, the displacement values of the pipeline

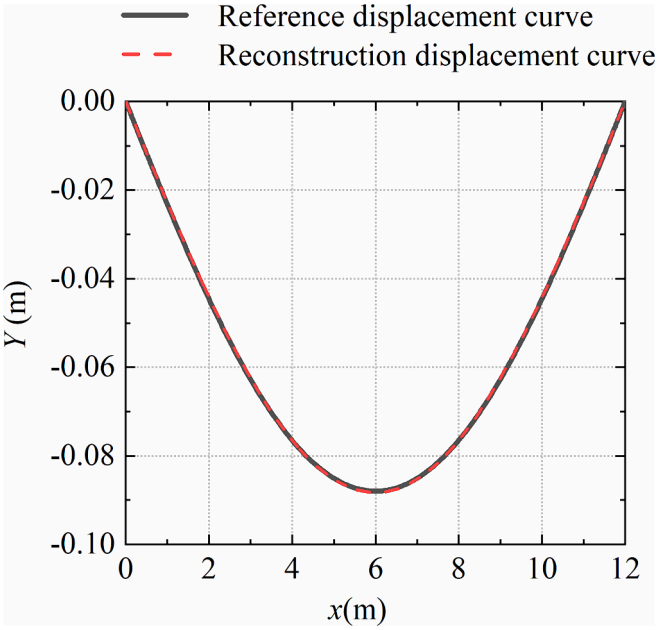

Fig. 5. Displacement distribution curve of simply supported pipeline at $t = 1$ s.

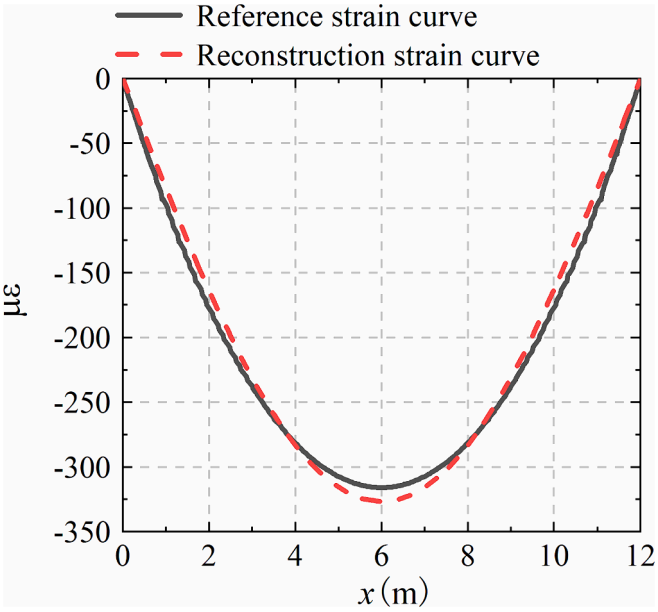

Fig. 6. Strain distribution curve of simply supported pipeline at $t = 1$ s.

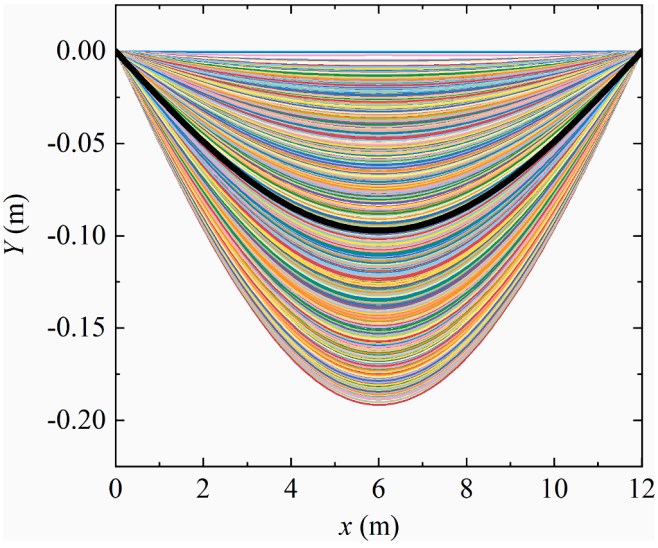

Fig. 7. Vibration displacement curves of pipeline within 0–5 s.

within 0–5 s are all negative. In the figure, the initial displacement of the pipeline is marked with a thick black line.

Second, the vibration acceleration data of several discrete measuring points within 0–5 s are collected, and the relative displacement generated by the vibration of each point is calculated using the displacement reconstruction algorithm. Taking the simulated vibration displacement data of each point as reference, the reconstructed displacement using acceleration is compared with the reference displacement to verify the feasibility of the displacement reconstruction algorithm. Fig. 8 shows the vibration displacement comparison curves of different points within 0–5 s.

The errors between the reconstruction displacement u and the reference displacement u_r of each measuring point within 0–5 s are shown in Table 1. In the table, Mean Relative Error(MRE) is the average of the relative differences between the observed values and the true values, calculated as:

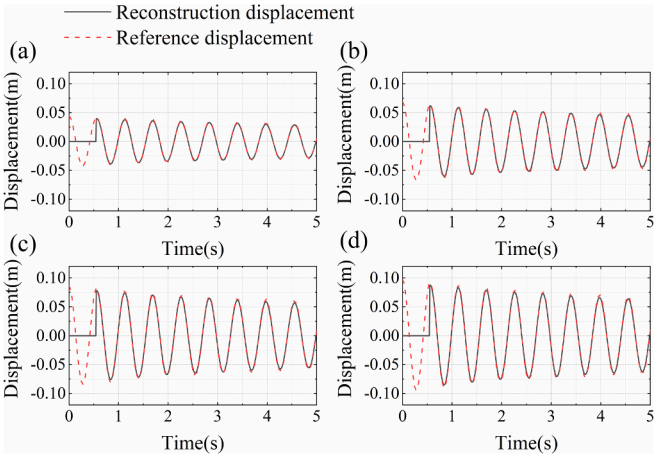

Fig. 8. Vibration displacement reconstruction comparison curves of different measuring points 0–5 s: (a) $x = 1.8$ m; (b) $x = 3$ m; (c) $x = 4.2$ m; (d) $x = 6$ m.

Table 1
Displacement reconstruction error of different measuring points within 0–5 s.

Measurement points	$x = 1.8$ m	$x = 3$ m	$x = 4.2$ m	$x = 6$ m
Mean Relative Error (%)	5.92	5.02	5.66	5.82
Mean Absolute Error (mm)	2.42	2.75	3.94	4.55
NRMSE (%)	5.86	4.98	5.60	5.75

$$MRE = \frac{1}{n}\frac{\Sigma|u - u_r|}{|u_r|}\# \tag{22}$$

wherein n is the number of sampling points for reconstructing the displacement curve, which is 446.

Mean Absolute Error (MAE) is defined as the average of the absolute differences between the observed values and the true values, and are calculated as:

$$MAE = \frac{1}{n}\Sigma|u - u_r|\# \tag{23}$$

Normalized Root Mean Square Error (NRMSE) is defined as the square root of the average squared differences between the observed values and the true values, and are calculated as:

$$NRMSE = \frac{\sqrt{\frac{1}{n}(u - u_r)2}}{u_{max^-}u_{min}}\# \tag{24}$$

It can be seen that the dynamic displacement curves inverted from acceleration data show good consistency with the reference displacement curves, with Mean Relative Error and NRMSE of both less than 6 %.

The relative displacement and initial displacement of each measuring point at $t = 2$ s, 3 s, 4 s and 5 s are superimposed. The simulated displacement curves with corresponding amplitudes are searched for matching in Fig. 7, and the results are shown in Fig. 9. The strain of the structure at the four moments are calculated and compared with the reference strain. And the results are shown in Fig. 10, where the reference strain is the strain at each given moment directly obtained from the simulation, and the reconstruction strain is the strain at the moment corresponding to the displacement curve obtained in the above matching process. Table 2 shows the comparison of the strains obtained from the displacement inversion at the four measuring points with the reference strain data. It can be seen that the overall average error between the inverse strain and the reference strain at each point is 7.22 %, and the maximum absolute error is 37 με.

Compared to the method of strain reconstruction based on the displacement–strain function, displacement matching can set exact load

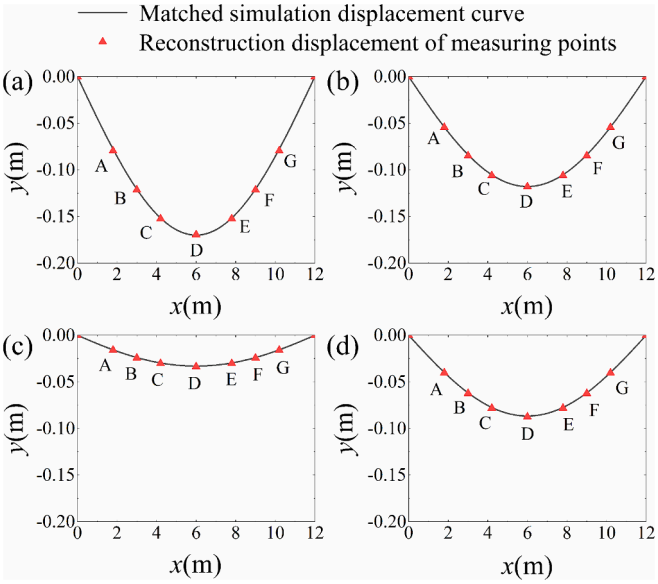

Fig. 9. Comparison of reconstructed displacement using acceleration data and successfully matched displacement curves at different times: (a) $t = 2$ s; (b) $t = 3$ s; (c) $t = 4$ s; (d) $t = 5$ s.

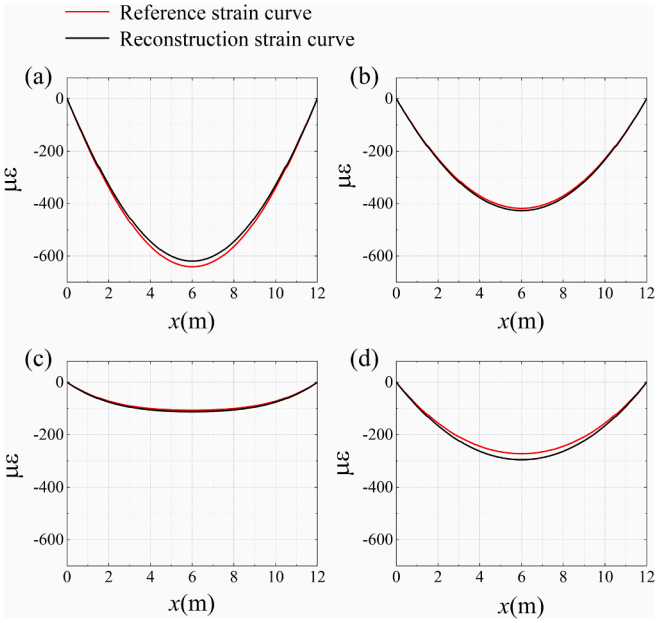

Fig. 10. Comparison of reconstructed strain curves at those moments when displacements are successfully matched and directly sampled strain curves at different times:(a) $t = 2$ s; (b) $t = 3$ s; (c) $t = 4$ s; (d) $t = 5$ s.

and boundary conditions in the model according to the actual situation, so the method has broader adaptability for complex structure and is used to reconstruct the strain of the structure in the following experiment to verify its effectiveness.

4. FBG accelerometer development

4.1. Design of FBG accelerometers

The FBG accelerometer adopts equal strength cantilever beam structure to make the FBG stretched evenly. The structure of the accelerometer is shown in Fig. 11. The length L_1, width b_1, thickness h, top

Table 2
Comparison of reconstructed and reference strains at different locations (με).

Time	$x = 1.8$ m		$x = 3$ m	
	Reconstructed strain	Reference strain	Reconstructed strain	Reference strain
1 s	−151	−162	−221	−239
2 s	−299	−309	−455	−470
3 s	−212	−208	−318	−311
4 s	−703	−648	−945	−861
5 s	−160	−143	−236	−208

Time	$x = 4.2$ m		$x = 6$ m	
	Reconstructed strain	Reference strain	Reconstructed strain	Reference strain
1 s	−266	−288	−291	−316
2 s	−559	−578	−619	−641
3 s	−387	−379	−426	−418
4 s	−106	−96	−112	−100
5 s	−284	−250	−310	−273

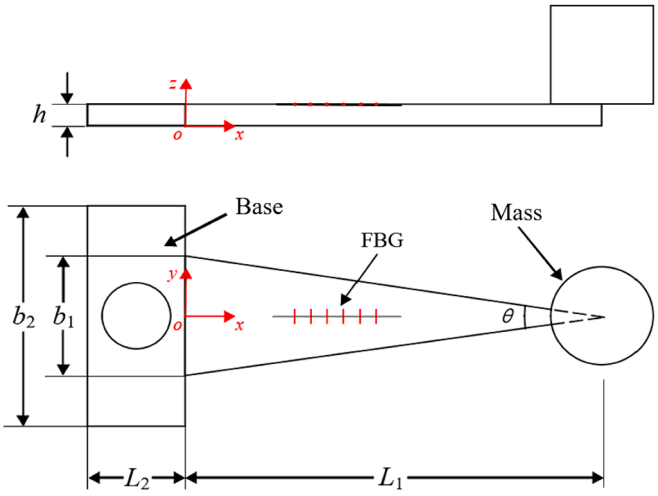

Fig. 11. Structure of FBG accelerometer with equal strength beam.

angle θ and elastic modulus E of the equal strength cantilever beam all affect the sensitivity and characteristic frequency of the accelerometer. The equal strength beam was modeled using the finite element simulation to determine the geometry parameters of the FBG accelerometer structure and the corresponding sensitivity and characteristic frequency. The natural frequency of large pipelines and bridges are usually very low, generally below 20 Hz. The first-order natural frequency of the designed accelerometer should be higher than 20 Hz to ensure a flat response of the accelerometer in the low frequency range.

According to parameter sweeping results in Fig. 12, it can be seen that the equal strength beam can maintain essentially uniform strain distribution over a wide range of top angle. The strain on the surface of the equal strength beam gradually decreases as θ increases, and the strain distribution begins to fluctuate greatly. When $\theta < 25°$, the strain distribution on the surface of the beam with equal strength is more uniform, and in the actual production, the top angle was selected as 20.25°.

Through simulation analysis, the dimensions of the FBG accelerometer were determined as $L_1 = 28$ mm, $L_2 = 10$ mm, $b_1 = 10$ mm, $b_2 = 20$ mm, $h = 0.3$ mm, and $M = 3$ g. According to the above dimensions, the FBG accelerometer was fabricated and packaged.

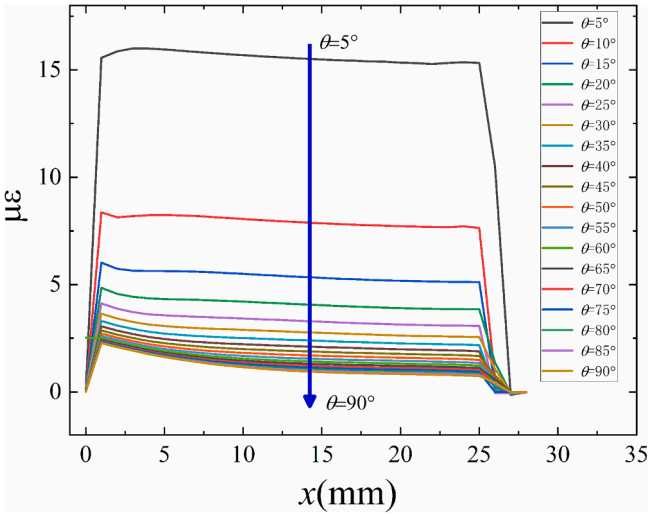

Fig. 12. Surface strain distribution of beams with equal strength under different top angle θ.

4.2. Testing of FBG accelerometers

The testing system of the fabricated FBG accelerometers is shown in Fig. 13. A vibration exciter was used to make the FBG accelerator vibrate, and a commercial accelerometer WT931 was used as the reference. The FBG accelerometer and reference accelerometer were attached to the same vibration platform of the exciter for calibration. The data of the center wavelength change of the FBG accelerometer during the vibration were extracted using an FBG demodulator and then transmitted to the computer for further processing.

Sensitivity sweep frequency test of the FBG accelerometer was carried out with a step size of 1 Hz. The amplitude-frequency response curve of the sensitivity is shown in Fig. 14. The resonant frequency of the accelerometer is 56 Hz, and the average sensitivity in the frequency range of 3 Hz–20 Hz is 70 pm·g^{-1}.

Linear responses of an FBG accelerometer were tested. The vibration signal of the shaker was set to 3 Hz and 20 Hz, and the acceleration was increased from 0.06 m/s^2 to 0.26 m/s^2, and the wavelength change of the FBG accelerometer was recorded during this process. Fig. 15 shows the linear response curves of acceleration obtained, and the wavelength change of the accelerometer has a good linear relationship with the input acceleration.

Several FBG accelerometers were fabricated according to the designed dimensions, followed by a consistency test. Fig. 16 shows the sensitivity amplitude-frequency response curves of five of those accelerometers. It can be observed that FBG accelerometers exhibit consistent sensitivity from 2 Hz–100 Hz. These FBG accelerometers will be used to measure the acceleration at different points on the vibrating beam.

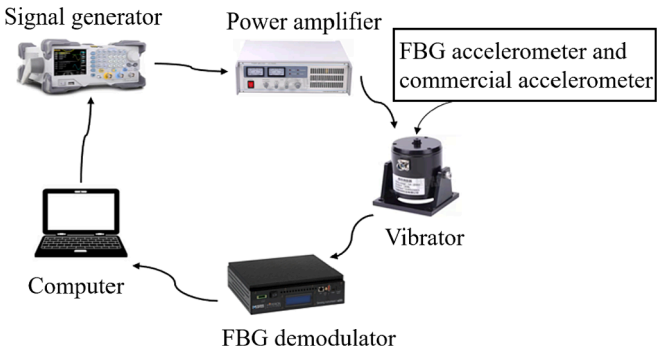

Fig. 13. FBG accelerometer test apparatus

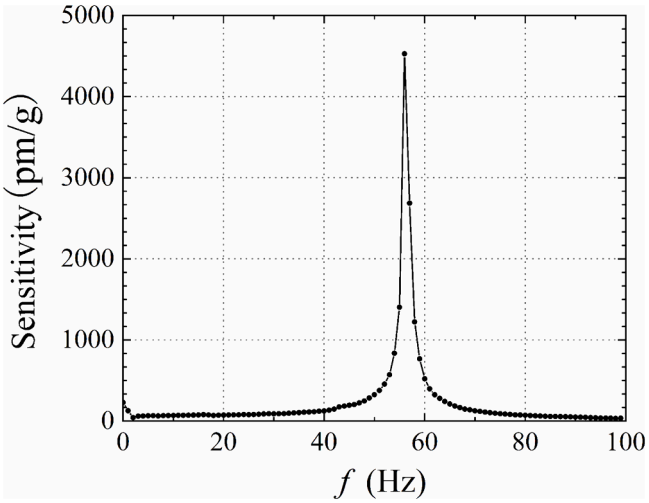

Fig. 14. Sensitivity amplitude-frequency response curve of one FBG accelerometer.

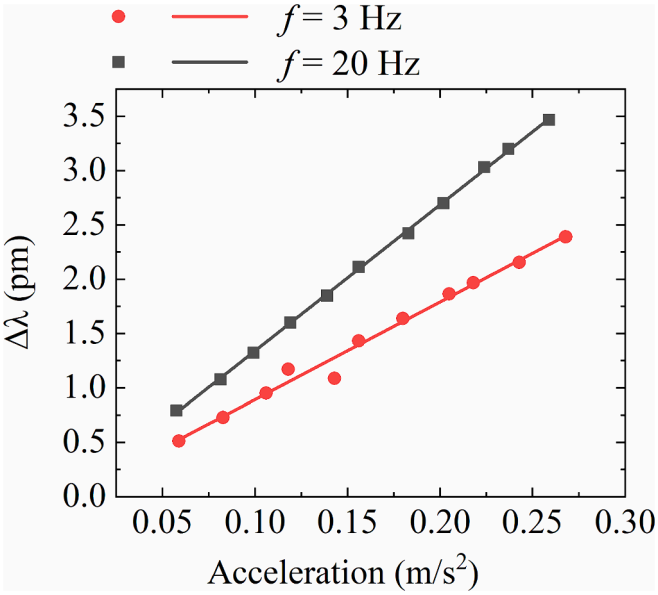

Fig. 15. Linear response curves of FBG accelerometer.

5. Experiment

5.1. Experiment method

The model of structural vibration shape monitoring system based on FBG accelerometer array is shown in Fig. 17, and experimental pipeline system is shown in Fig. 18. Among them, force F was applied to the pipeline structure to induce dynamic deformation. The FBG accelerometers were used to measure the acceleration at different points. The FBG strainmeter measured the strain at different points, which was used as the reference strain. The distributed strain of the pipeline based on the acceleration information inversion would be compared with the reference strain to verify the feasibility and accuracy of the proposed method.

Besides, the FBG dynamic strain demodulator Si255 was used to demodulate the central wavelength signals of each FBG accelerometer and strainmeter. The laser displacement sensor AM-D100 with the measuring accuracy of 0.01 mm was used to verify the accuracy of displacement reconstruction of the system. The output of the laser displacement sensor was collected using synchronous data acquisition

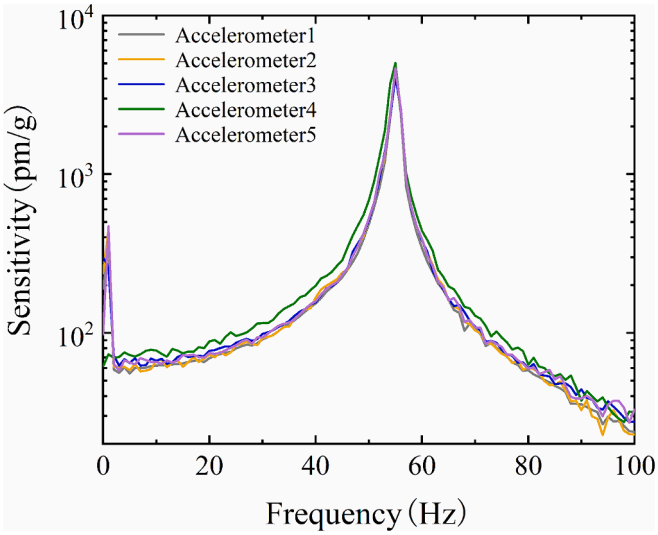

Fig. 16. Sensitivity amplitude-frequency response curves of five developed FBG accelerometers.

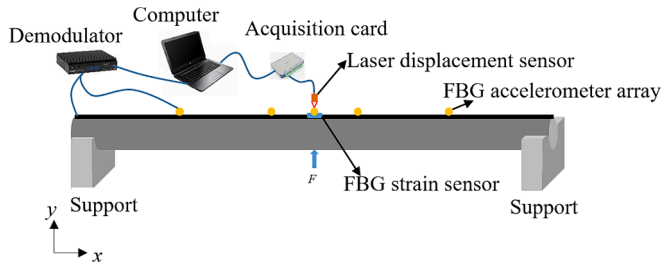

Fig. 17. Experimental system schematic of pipeline vibration shape monitoring.

card Smacq's USB-5700. At the same time, the output signals of the FBG demodulator and acquisition card were transmitted to the computer through the network port and serial port respectively, and the LabVIEW software installed on the computer realized the signal processing and display functions for the monitoring of structural vibration shape.

5.2. Results and discussions

The displacement–strain reconstruction experiment was carried out on an actual steel pipeline. The FBG accelerometers were deployed on the surface of the pipeline as shown in Fig. 18. An instantaneous force was used to knock the center of the pipeline to make it vibrate. Three laser displacement sensors were used to monitor the displacements at three measurement points as reference. The computer was used to collect the acceleration data of each point and carry out displacement reconstruction, and the reconstructed displacement curves were compared with the curves from the laser displacement sensors.

Fig. 19 respectively shows the displacement curves comparison of measuring points at $x = 2.4$ m, 4.8 m and 6 m. It can be seen that the reconstruction displacement is in good agreement with the reference displacement. The average errors at each peak between the reference displacement curve and the reconstructed displacement curve at different measurement points are calculated, and the results are shown in Table 3. It can be seen that the maximum Mean Relative Error of the displacement curve is 7.61 %, and the maximum NRMSE is 8.26 %.

Another three groups of experiments were carried out. In each group of experiment, the pipeline was stricken with different strengths at its center to cause vibration. In each group of experiments, the vibration displacement reconstruction curve at each point on the pipeline surface

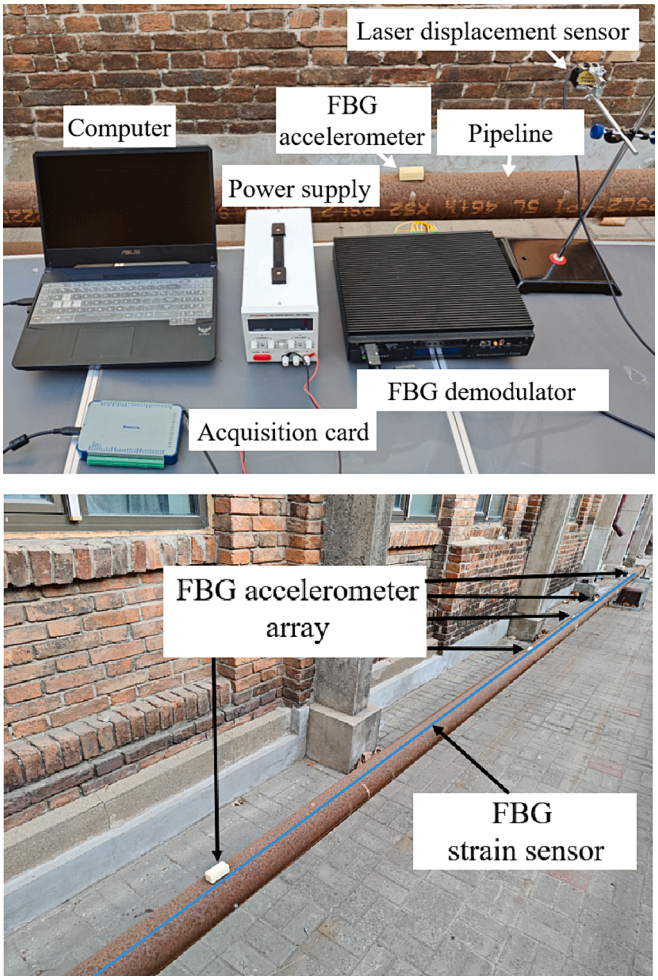

Fig. 18. Experimental pipeline system.

was calculated, recorded and then matched with the simulation displacement curve at each moment. During the matching process, the time point where the error between simulated displacement and reconstructed displacement was minimized can be found. The simulated strain at that time point is considered as the reconstructed strain of the structure. The reference strain at the pipeline center point could be measured by the FBG strainmeter attached to the surface of the pipeline. The displacements of the two support ends of the pipeline were set to zero. The vibration displacement reconstruction curves of discrete points in each group, along with the comparison between reconstruction displacement and matched simulation displacement are shown in Fig. 20. The errors comparison between the reference strain and the reconstruction strain are shown in Table 4. From Table 4, it can be seen that the maximum relative error between the reference strain and the reconstruction strain is 10.8 %.

In Fig. 20, the maximum value of each vibration cycle of the displacement reconstruction curves is utilized for matching, which is equivalent to 11 repeated measurements in each experiment. The experimental standard deviation of strain is as follows:

$$S_\varepsilon = \sqrt{\frac{\sum_{i=1}^{n}(\varepsilon_i - \bar{\varepsilon})^2}{n-1}}\# \tag{25}$$

wherein ε_i is the strain for each measurement, $\bar{\varepsilon}$ is the mean value of measured strain, and n is the number of measurements. The experimental standard deviation of the mean strain is as follows:

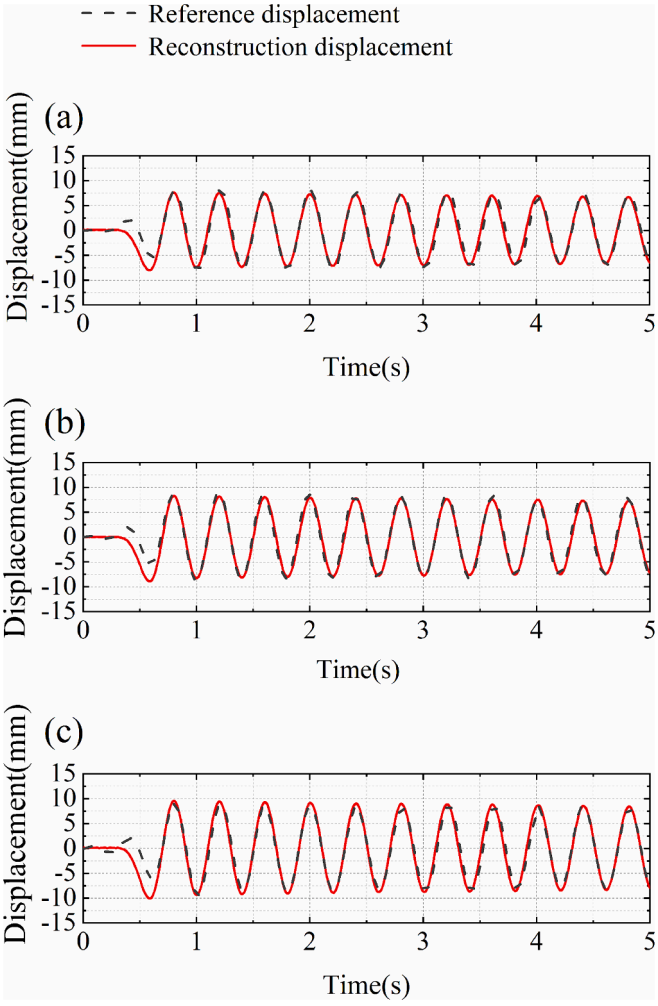

Fig. 19. Comparison of reconstructed vibration displacements and reference displacements measured by laser sensors at (a) $x = 2.4$ m; (b) $x = 4.8$ m; (c) $x = 6$ m.

Table 3
Errors of pipeline vibration displacement reconstruction.

Position	$x = 2.4$ m	$x = 4.8$ m	$x = 6$ m
Mean Relative Error (%)	7.61	6.13	7.57
Mean Absolute Error (mm)	0.72	0.60	0.71
NRMSE (%)	8.26	6.66	8.18

$$\overline{S_\varepsilon} = \frac{S_\varepsilon}{\sqrt{n}}\# \tag{26}$$

Type A evaluation of measurement uncertainty of strain is as follows:

$$U_A = t_p\overline{S_\varepsilon}\# \tag{27}$$

Taking a confidence level of $P = 95$ % and $n = 11$, according to the t-distribution table, it can be concluded that$t_p = 2.23$. Using the above formula, it can be calculated that at a 95 % confidence level, the maximum measurement uncertainty of the proposed method is 2.21 με.

Currently, there is a certain degree of errors between the reference strain and the reconstructed strain, and this is primarily due to possible discrepancies between the models established in the finite element simulation and existing in the actual conditions. To further improve accuracy, it is important to establish a model that closely mimic the actual conditions by considering materials, load, boundary conditions, and other relevant factors.

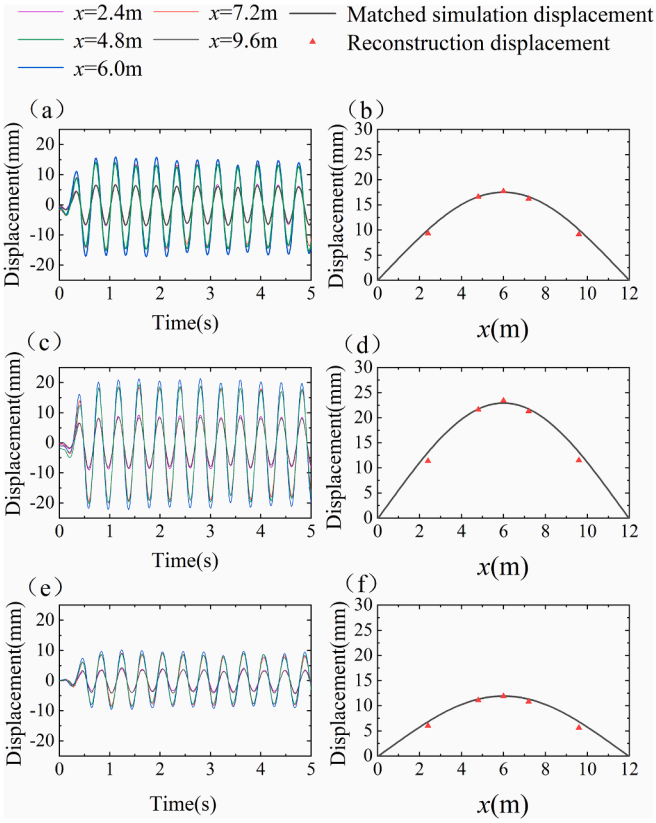

Fig. 20. Experimental results of pipeline displacement reconstruction: (a)(c)(e) displacement reconstruction curves at five points; (b)(d)(f) comparison between the reconstructed displacement and the matched displacement from simulation curves.

Table 4
Strain reconstruction error of pipeline vibrating test.

Experiment number	Reconstruction strain/ με	Reference strain/ με	Relative error
1	63.7	68.4	6.87 %
2	80.5	90.3	10.8 %
3	42.6	46.7	8.69 %

The second factor in the error is the effect of temperature on the FBG accelerator accuracy. The temperature at which the FBG accelerometer is calibrated is different from that at which it is applied in the pipeline. The central wavelength of FBG will drift with the change of temperature, which will cause the sensitivity of FBG acceleration to change, and the measurement results of acceleration are inaccurate. The deviation of acceleration measurement will eventually lead to the deviation of strain reconstruction. This can be done by adding a reference FBG inside the FBG accelerometer or by using differential FBG to eliminate the effect of temperature drift.

Additionally, the FBG accelerometers developed by this paper can only measure acceleration in one-dimensional direction. Further research could turn to the design of multi-axis FBG accelerometers to effectively detect the vibration displacement and shape of objects in multiple directions. In this way, more vibration characteristics can be extracted and more accurate strain information can be reconstructed. In addition to that, errors between the reference strain and the reconstructed strain also arise from the calibration of accelerometers and the displacement reconstruction algorithm. By improving the accuracy of both the calibration and algorithm, it is possible to reduce the errors as well.

6. Conclusions

This paper proposes a displacement and distributed strain reconstruction method based on FBG accelerometers for vibrating structure where direct attachment of FBG strainmeter on the surface is not feasible. The main research contents and conclusions are as follows:

(1) Displacement reconstruction method based on FIR filter is studied, where vibration acceleration at discrete points on the structure surface is extracted to reconstruct displacement. A method of obtaining the strain distribution by matching the reconstructed displacement with that obtained via finite element simulation is proposed. Compared with displacement–strain function from vibratory beam theory, the displacement matching method via finite element simulation has higher strain reconstruction accuracy and broader adaptability. The total mean relative error at all points is less than 6 %, and the total relative error of inversion strain at all points is less than 9 %.
(2) An FBG accelerometer with equal strength beam structure is designed and optimized by geometric parameter sweeping. Excitation test shows that the resonant frequency of the FBG accelerometer is 56 Hz, the average sensitivity in 3 Hz–20 Hz is 70 $pm \cdot g^{-1}$, and the FBG accelerometer demonstrates good linearity.
(3) A pipeline vibration monitoring experiment system is built, and displacement–strain reconstruction experiment is carried out. Experiment results demonstrate that the proposed method has a high detection accuracy, with the maximum relative error of displacement reconstruction being 7.6 %, and the maximum relative error of strain reconstruction being 10.8 %. The maximum measurement uncertainty of the proposed method at a confidence level of 95 % is 2.21 με.

CRediT authorship contribution statement

Huang Xinjing: Conceptualization, Methodology, Investigation, Funding acquisition, Supervision, Resources, Project administration, Writing - review & editing. **Zhang Zhipeng:** Data curation, Investigation, Writing - original draft, Writing - review & editing. **Cheng Tongyao:** Validation, Supervision, Visualization, Writing - original draft. **Li Jian:** Resources, Software, Supervision. **Ma Jinyu:** Conceptualization, Methodology, Data curation, Formal analysis, Software, Validation, Visualization.

Declaration of competing interest

The authors declare that they have no known competing financial interests or personal relationships that could have appeared to influence the work reported in this paper.

Data availability

Data will be made available on request.

Acknowledgments

This work is supported by National Natural Science Foundation of China under Grant 62073233, Natural Science Foundation of Tianjin under Grant 21JCQNJC00690.

References

[1] S. Alessandro, Pedestrian bridge vibration monitoring using a wireless MEMS accelerometer board, in: IEEE 19th International Conference on Computer Supported Cooperative Work in Design (CSCWD), IEEE, Calabria, Italy, 2015, p. 2015.
[2] K. Yüksel, D. Kinet, V. Moeyaert, et al., Railway monitoring system using optical fiber grating accelerometers, Smart Mater. Struct. 27 (10) (2018) 105033.
[3] S.H. Crandall, W.D. Mark, Random Vibration in Mechanical Systems, 1963.
[4] Paulo Fernando Da Costa Antunes, Hugo F.T. Lima, Nélia Jordão Alberto et al., Optical fiber accelerometer system for structural dynamic monitoring, IEEE Sens. J. 9 (11) (2009) 1347–1354.
[5] X. Gong, Y. Kuo, W. Liao, et al., An aerosol deposition based MEMS piezoelectric accelerometer for low noise measurement, Microsyst. Nanoeng. 9 (1) (2023) 23.
[6] X. Han, P. Wang, D. Cui, et al., Rebar corrosion detection in concrete based on capacitance principle, Measurement 209 (2023) 112526.
[7] B. Glisic, Y. Yao, S.-T. Tung, et al., Strain sensing sheets for structural health monitoring based on large-area electronics and integrated circuits, Proc. IEEE 104 (8) (2016) 1513–1528.
[8] F. Mumtaz, M. Roman, B. Zhang, et al., Assembly-free ultra-sensitive miniaturized strain sensor based on an asymmetric optical fiber taper, Measurement 211 (2023) 112655.
[9] A. Baggio, M. Turani, M. Olivero, et al., Selective distributed optical fiber sensing system based on silicone cladding optical fiber and Rayleigh backscattering reflectometry for the detection of hydrocarbon leakages, Opt. Laser Technol. 161 (2023) 109158.
[10] Wu. Huifeng, R. Dong, Z. Liu, et al., Deformation monitoring and shape reconstruction of flexible planer structures based on FBG, Micromachines 13 (8) (2022) 1237.
[11] A.O. Soge, O.F. Dairo, M.E. Sanyaolu, et al., Recent developments in polymer optical fiber strain sensors: a short review, J. Opt. 50 (2) (2021) 299–313.
[12] H. Wang, P. Xiang, L. Jiang, Strain transfer theory of industrialized optical fiber-based sensors in civil engineering: a review on measurement accuracy, design and calibration, Sens. Actuat., A 285 (2019) 414–426.
[13] G. Ding, X. Yan, X. Gao, et al., Reconstruction of propeller deformation based on FBG sensor network, Ocean Eng. 249 (2022) 110884.
[14] J. Frieden, J. Cugnoni, J. Botsis, et al., High-speed internal strain measurements in composite structures under dynamic load using embedded FBG sensors, Compos. Struct. 92 (8) (2010) 1905–1912.
[15] X. Song, D. Liang, Dynamic displacement prediction of beam structures using fiber bragg grating sensors, Optik 158 (2018) 1410–1416.
[16] T. Li, L. Qiu, H. Ren, Distributed curvature sensing and shape reconstruction for soft manipulators with irregular cross sections based on parallel dual-FBG arrays, IEEE/ASME Trans. Mechatron. 25 (1) (2019) 406–417.
[17] Hae Sung Lee, Yun Hwa Hong, Hyun Woo Park, Design of an FIR filter for the displacement reconstruction using measured acceleration in low-frequency dominant structures, Int. J. Numer. Meth. Eng. 82 (4) (2010) 403–434.
[18] W. Zheng, D. Dan, W. Cheng, et al., Real-time dynamic displacement monitoring with double integration of acceleration based on recursive least squares method, Meas.: J. Int. Meas. Confed. 141 (2019) 460–471.
[19] H. Zhu, Y. Zhou, Hu. Yumei, Displacement reconstruction from measured accelerations and accuracy control of integration based on a low-frequency attenuation algorithm, Soil Dyn. Earthq. Eng. 133 (2020) 106122.
[20] H. Kwon, Y. Park, C. Shin, et al., In-flight strain monitoring of aircraft tail boom structure using a fiber Bragg grating sensor based health and usage monitoring system, Int. J. Aeronaut. Space Sci. 22 (3) (2021) 567–577.
[21] M. Mieloszyk, K. Majewska, W. Ostachowicz, Application of embedded fibre Bragg grating sensors for structural health monitoring of complex composite structures for marine applications, Mar. Struct. 76 (2021) 102903.
[22] P. Antunes, H. Varum, P. André, Uniaxial fiber Bragg grating accelerometer system with temperature and cross axis insensitivity, Measurement 44 (1) (2011) 55–59.
[23] N. Gutiérrez, P. Galvín, F. Lasagni, Low weight additive manufacturing FBG accelerometer: design, characterization and testing, Measurement 117 (2018) 295–303.
[24] Q. Liu, X. Qiao, Fu. Haiwei, et al., Large frequency range and high sensitivity fiber Bragg grating accelerometer based on double diaphragms, IEEE Sens. J. 14 (5) (2014) 1499–1504.
[25] F. Zhang, S. Jiang, C. Wang, et al., Broadband and high sensitivity FBG accelerometer based on double diaphragms and h-shaped hinges, IEEE Sens. J. 21 (1) (2020) 353–359.
[26] M.D. Todd, G.A. Johnson, B.A. Althouse, et al., Flexural beam-based fiber Bragg grating accelerometers, IEEE Photon. Technol. Lett. 10 (11) (1998) 1605–1607.
[27] A Mita, I Yokoi, Fiber Bragg grating accelerometer for structural health monitoring, in: Fifth International Conference on Motion and Vibration Control (MOVIC 2000), Sydney, Australia, 2000.
[28] Y. Weng, X. Qiao, Z. Feng, et al., Compact FBG diaphragm accelerometer based on L-shaped rigid cantilever beam, Chin. Opt. Lett. 9 (10) (2011) 100604.
[29] K.-S. Lim, M.K.A. Zaini, Z.-C. Ong, et al., Vibration mode analysis for a suspension bridge by using low-frequency cantilever-based FBG accelerometer array, IEEE Trans. Instrum. Meas. 70 (8) (2020) 1–8.
[30] Y. Weng, X. Qiao, T. Guo, et al., A robust and compact fiber Bragg grating vibration sensor for seismic measurement, IEEE Sens. J. 12 (4) (2012) 800–804.
[31] N. Basumallick, I. Chatterjee, P. Biswas, et al., Fiber Bragg grating accelerometer with enhanced sensitivity, Sens. Actuat., A 173 (1) (2012) 108–115.
[32] Q. Liu, X. Qiao, J. Zhao, et al., Novel fiber bragg grating accelerometer based on diaphragm, IEEE Sens. J. 12 (10) (2012) 3000–3004.
[33] Z. Zhang, C. Liu, H. Li, et al., Optical fiber grating vibration sensor for vibration monitoring of hydraulic pump, Photon. Sens. 7 (2) (2017) 140–147.